Optics Letters

Optical power detector with broad spectral coverage, high detectivity, and large dynamic range

Jussi Rossi,[1,*] Juho Uotila,[2] Sucheta Sharma,[3] Tuomas Hieta,[4] Toni Laurila,[3] Roland Teissier,[5] Alexei Baranov,[5] Erkki Ikonen,[3,6] and Markku Vainio[1,7]

[1]Photonics Laboratory, Physics Unit, Tampere University, Tampere, Finland
[2]Patria Aviation Oy, Tampere, Finland
[3]Metrology Research Institute, Aalto University, Espoo, Finland
[4]Gasera Ltd., Turku, Finland
[5]IES, University of Montpellier, CNRS, Montpellier, France
[6]VTT MIKES, Espoo, Finland
[7]Department of Chemistry, University of Helsinki, Helsinki, Finland
*Corresponding author: jussi.rossi@tuni.fi

Received 9 February 2022; revised 3 March 2022; accepted 4 March 2022; posted 4 March 2022; published 25 March 2022

Optical power measurements are needed in practically all technologies based on light. Here, we report a general-purpose optical power detector based on the photoacoustic effect. Optical power incident on the detector's black absorber produces an acoustic signal, which is further converted into an electrical signal using a silicon-cantilever pressure transducer. We demonstrate an exceptionally large spectral coverage from ultraviolet to far infrared, with the possibility for further extension to the terahertz region. The linear dynamic range of the detector reaches 80 dB, ranging from a noise-equivalent power of 6 $nW/\sqrt{Hz}$ to 600 mW (independent of signal averaging time).

Published by Optica Publishing Group under the terms of the Creative Commons Attribution 4.0 License. Further distribution of this work must maintain attribution to the author(s) and the published article's title, journal citation, and DOI.

https://doi.org/10.1364/OL.455191

Power detector is one of the most important components in technologies based on light or other electromagnetic radiation. Depending on the application, typical detector parameters of interest include noise-equivalent power (NEP), linear dynamic range, speed, spectral coverage, and ease of use. Semiconductor photodetectors, such as Si photodiodes, provide excellent performance with respect to many of these parameters, but the spectral coverage is limited on the long-wavelength side by the bandgap energy of the detector material. Although extension to long wavelengths is in some cases possible by material engineering, the reduced bandgap inevitably leads to increased thermal noise and thus to the need for cooling of the detector, even down to cryogenic temperatures [1]. In practice, the responsivity of a typical state-of-the-art HgCdTe (MCT) infrared detector sharply rolls off at approximately 12 μm [2]. Beyond that, thermal detectors are often used. In a thermal detector, a black material absorbs the incoming optical radiation and the resulting temperature increase of the material is measured [2]. An advantage common to all thermal detectors is that they can be made practically wavelength independent [3]. This allows access to the long infrared part of the electromagnetic spectrum, which is becoming increasingly important due to numerous applications based on molecular spectroscopy and thermal imaging: a trend that is catalyzed by the fast development of coherent infrared light sources [4,5].

The most common thermal detectors include bolometers, pyroelectric detectors, and thermopiles, all of which use temperature dependence of an electric property of the detector material [2,6]. The photoacoustic (PA) effect offers an alternative approach [7]. In the PA effect, the temperature increase due to absorption of the incident electromagnetic radiation induces a pressure change in the surrounding gas. If the incident radiation is modulated, similar to what is done with, e.g., pyroelectric detectors, the temperature change and the corresponding pressure change become periodic [Fig. 1(a)]. That is, an acoustic signal directly proportional to the absorbed power is produced. The acoustic signal can be converted into an electrical signal by a sensitive microphone.

The photoacoustic detection principle is versatile and tailorable for various applications. As an example, ultrasound transducers that operate at MHz frequencies provide high spatial resolution in fast photoacoustic imaging in medical applications [8,9]. However, some of the best detection limits in gas-phase molecular spectroscopy have been obtained by optimizing the detection at lower (10 Hz to 100 kHz) acoustic frequencies [10,11], an approach that has recently opened new avenues also in broadband laser spectroscopy [12]. The use of the PA effect in optical power detection has been known from the 1940's, when Golay developed a photoacoustic cell particularly designed for this purpose [13]. The Golay cell is one of the best thermal detectors in terms of detection sensitivity, but its diaphragm microphone is fragile and susceptible to technical noise caused by mechanical vibrations [6]. The dynamic range of the diaphragm microphone is also modest, limiting the measurable optical power range to approximately 100 nW to 1 mW for an optimized commercially available instrument

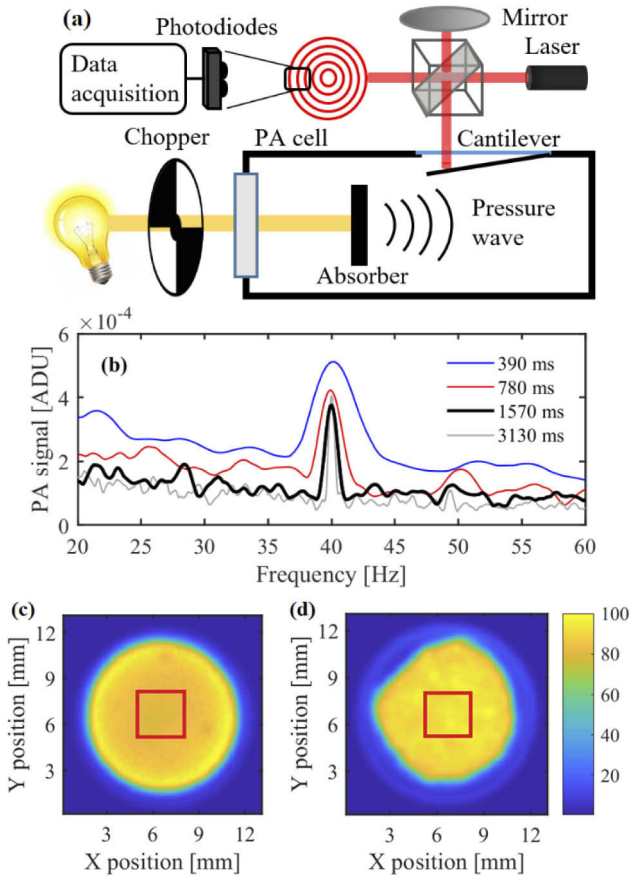


Fig. 1. (a) Simplified schematic of the PA power detector. (b) Examples of PA spectra obtained by FFT of the cantilever signal. The spectrum shows the PA noise floor and, on top of that, the actual signal at the modulation frequency (40 Hz). Signal peaks are recorded with different measurement times (FFT time constants) and with 50 nW of incident optical power at $\lambda = 633$ nm. ADU = arbitrary detector units. (c) Spatial PA response of the soot absorber and (d) of the CNT absorber. The red squares show the 3 mm × 3 mm areas used in spatial uniformity calculations, see Supplement 1 for details.

[14]. The measurement range can be shifted toward lower powers, and NEP values of close to or below 1 nW/$\sqrt{\text{Hz}}$ have been reported for both Golay cells and miniaturized versions based on tunneling displacement transducers [6,15]. The poor linearity of the diaphragm microphone poses an additional challenge [16,17]. Due to these limitations, the Golay cell mainly finds use in niche laboratory applications, although the fundamental underlying principle, photoacoustic detection, offers the possibility for one of the most versatile high-performance thermal detectors.

In this Letter, we introduce a novel photoacoustic power detector that surpasses the linear dynamic range of the Golay cell and other common infrared detectors by several orders of magnitudes, while offering excellent stability, rugged construction, and ease of use. Our solution is based on a silicon-cantilever acoustic sensor, which has previously been used to realize some of the most sensitive methods ever developed for optical gas analysis [10,18,19]. Here, to the best of our knowledge, we show for the first time that the same fundamental principle can lead to a simple and universal electromagnetic power detector that works virtually at any wavelength without cooling, thus benefiting a wide range of applications. While the main motivation of our work is to develop a general-purpose optical power detection method, the work also contributes to the development of traceable power measurements in the long-wavelength infrared and terahertz (THz) regions, where power calibrations are particularly difficult to carry out. An elegant solution proposed for reduction of the uncertainty of such calibrations is to link the long-wavelength power responsivity scale to a more accurate responsivity scale in the visible spectral range [20]. This requires a reference detector with broad spectral coverage and predictable spectral responsivity. Other potential uses of the new detector technology include broadband infrared spectroscopy [12], atmospheric monitoring and trace gas sensing [21], nanomaterial characterization [22], as well as infrared imaging with applications in health, safety, and security [23,24].

The operating principle of the cantilever-enhanced power detector is shown schematically in Fig. 1(a). The radiation incident on the detector is first modulated with a mechanical chopper and then focused on the absorber inside of a sealed photoacoustic cell (see Supplement 1 for details of the components). Due to the large diameter (≥10 mm) of both the cell window and the absorber, the detector is also suitable for measurements of incoherent radiation and long wavelengths. The PA cell is filled with an acoustic carrier gas, such as N_2 or He, which are optically transparent gases with a small number of internal degrees of freedom and thus provide a strong photoacoustic response without compromising the flatness of the spectral response [25,26]. The acoustic wave generated by modulated absorption is detected by a silicon cantilever [18]. It is mechanically robust and suitable for field applications despite being only a few micrometers thick [27]. The cantilever deflection is measured at picometer resolution using a compact laser-interferometric readout module that produces an electrical signal. The signal is recorded by monitoring the signal peak in the photoacoustic frequency spectrum [Fig. 1(b)] that is obtained from the digitized interferometer signal in real time by fast Fourier transform (FFT). The signal-to-noise ratio (SNR) depends on the FFT time constant (averaging time) as demonstrated in Fig. 1(b). The vertical axis is shown in raw units of the PA signal, arbitrary detector units (ADU), which is directly proportional to the measured optical power. The same comparable units are also used elsewhere in this Letter.

Unlike with many other photoacoustic [8,11] or photothermal [28,29] sensors, the acoustic frequency of cantilever-enhanced PA detection can be chosen freely; there are no acoustic resonances [25] that would require precise matching of the modulation frequency with a narrow acoustic resonance of the cell. This property simplifies the detector design and, as is shown below, gives an additional method to increase the dynamic range of PA detection. With the cantilever used in this work, the best SNR is obtained at modulation frequencies of the order of 40 Hz [25].

The proof-of-concept study reported here covers a wide range of wavelengths, from 325 nm to 25 μm. We have previously carried out rigorous characterization of the photoacoustic properties of several black absorber materials using the same experimental setup [25], based on which we have chosen a simple absorber fabricated in-house by depositing candle soot on an aluminum substrate, as well as a commercially available carbon nanotube (CNT) sample. The soot-based absorber gives a larger PA signal while the CNT absorber has a flatter spectral

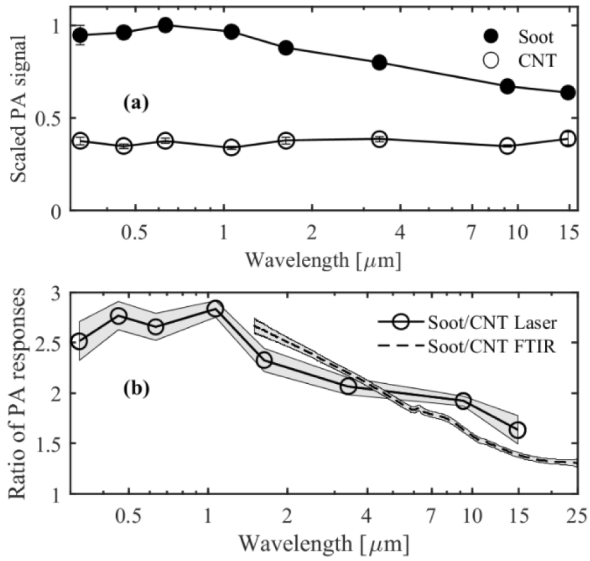


Fig. 2. (a) Spectral responsivity of the PA detector measured with two different absorbers at discrete laser wavelengths. (b) Comparison of the two absorbers, soot on aluminum and a CNT sample. The dashed line between wavelengths 1.5 and 25 μm is measured with an incandescent light source and a Fourier-transform infrared (FTIR) spectrometer. The individual data points from 325 nm to 14.85 μm are recorded with lasers. The slight discrepancy between these two datasets is due to a frequency-dependent artifact in the FTIR measurements (see Supplement 1).

response; see Fig. 2(a). The dashed-line plot in Fig. 2(b) was measured with a broadband thermal light source, while the individual dots summarize the results of laser-based calibrations at several wavelengths, from 325 nm to 14.85 μm. Measurement uncertainty estimates are shown in the figures with error bars, see Supplement 1 for details.

One of the advantages of the cantilever microphone is its excellent linear dynamic range. The linearity of a conventional microphone is limited by the nonlinear stretching of the diaphragm. An additional nonlinear contribution arises from the electrostatic forces if capacitive readout of the microphone signal is used. The silicon cantilever is attached to its frame from only one side, which results in a highly linear motion that is precisely monitored by the interferometric readout unit. The large linear dynamic range of 60 dB is exemplified in Figs. 3(a) and 3(c). With the soot-based absorber and He as the acoustic carrier gas, the normalized NEP measured at 1064 nm is 5.6 $\mathrm{nW}/\sqrt{\mathrm{Hz}}$, corresponding to a specific detectivity of $D^* = 1.6 \times 10^8\ \mathrm{cm}\sqrt{\mathrm{Hz}}/\mathrm{W}$. We have experimentally confirmed that, unlike with most other optical detectors, the detector noise and the PA response are independent of the absorber size or the laser spot diameter, the latter of which we varied from 1 to 3 mm. The NEP and D^* compare favorably to state-of-the-art uncooled mid-infrared detectors, such as pyroelectric detectors coated with carbon nanotubes [30,31]. The upper limit (8.2 mW at 40 Hz modulation frequency) of the dynamic range is in this case set by saturation of the readout interferometer. This linear dynamic range is at least 20 dB better than that of a typical MCT detector [32] or Golay cell [16] and can be further enhanced by varying the modulation frequency, because the photoacoustic response drops as the modulation frequency is increased

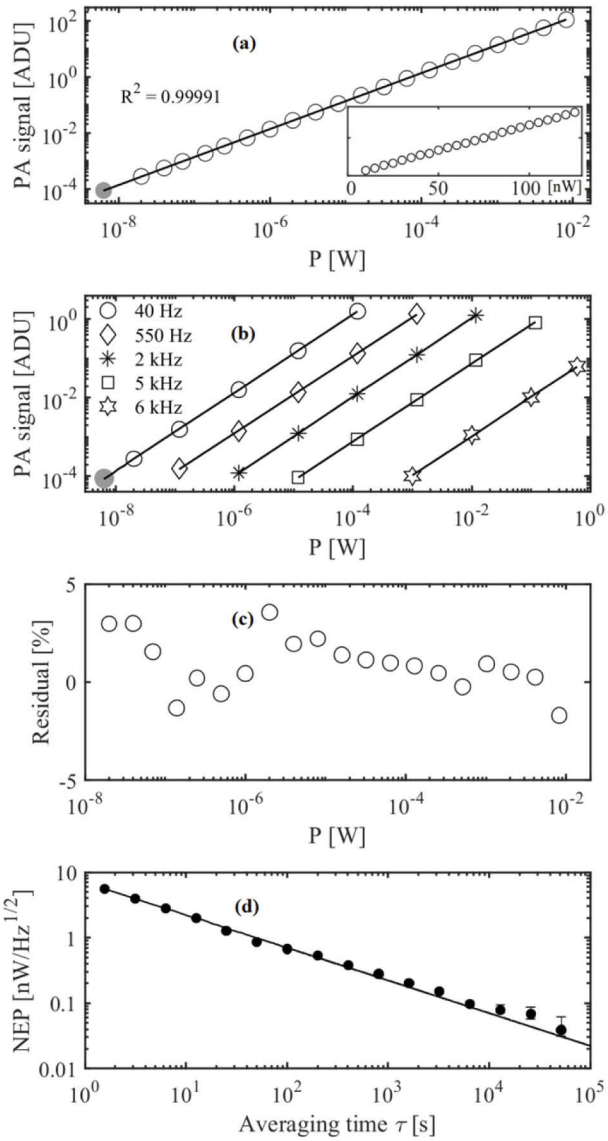


Fig. 3. Linearity and NEP of the photoacoustic power detector using soot-based absorber. (a) The circles indicate the measured PA signal as a function of incident optical power at a wavelength of 1064 nm, measured with an averaging time of 1.57 s and a modulation frequency of 40 Hz. Solid gray dot indicates the noise-equivalent power at a modulation frequency of 40 Hz and the solid line is a linear fit to the data. The inset shows low-power points on a linear scale. (b) Extension of the linear dynamic range by adjustment of the chopping frequency up to 6 kHz. (c) The relative residual of panel (a), i.e., the relative deviation of the measured points from the linear fit. (d) Dependency of the detector NEP on the averaging time τ. The straight line indicates the white-noise slope $\tau^{-1/2}$ of Allan deviation.

[25]. Alternatively, one can avoid signal saturation by reducing the chopping duty cycle, which limits the amount of optical energy incident on the detector per pulse. These techniques allowed us to extend the maximum measurable power on the fly to over 600 mW without saturating the detector [Fig. 3(b), Supplement 1]. As a result, we achieve a total linear dynamic range of 80 dB with a detection bandwidth of 1 Hz.

As mentioned above, PA detection can be designed for different data acquisition speeds. General power measurements tend to require a low detection limit but not a fast response time, for which reason we have designed the setup for low modulation frequencies. We typically use a measurement time (FFT time constant) of 1.57 s, although much shorter times are possible, as illustrated in Fig. 1(b). Also note that by increasing the chopping frequency up to several kHz [Fig. 3(b)], one can reduce the measurement time down to the millisecond level. However, some applications can use even longer averaging times, benefitting from the excellent stability and white-noise limited performance that are demonstrated in Fig. 3(d).

In summary, we have demonstrated a next-generation photoacoustic power detector that is based on a robust silicon-cantilever microphone, is easy to use, and works without cooling. Our proof-of-concept device works from ultraviolet to long infrared wavelengths, significantly exceeding the spectral coverage of semiconductor photodetectors. Owing to the fundamental wavelength-independent nature of the photoacoustic effect, further extension to the THz region is possible by optimizing the absorber and window material of the cell. Together with the excellent linear dynamic range, the wavelength-independent concept is appealing not only for general purposes but also for the development of power meters and transfer standards that can reduce the uncertainty of long-wavelength power measurements (given that rigorous metrological characterization of the detector is first done over the entire spectral range). The strength of the PA signal scales favorably with smaller acoustic cell size, which together with the compact cantilever microphone offers room for substantial miniaturization of the instrument. Further miniaturization may be achieved by applying the light-absorbing coating directly on the cantilever, in which case the detection would be based on the photothermal (thermoelastic) effect instead of the photoacoustic effect. In addition to super-resolution microscopy, such an approach was recently proposed for optical power detection by quartz tuning forks [28,29]. However, our present concept is ideal for the detection of thermal light and long-wavelength radiation because the absorber diameter can be made large without compromising the measurement SNR.

Funding. Academy of Finland (314364, 320165, 320167, 326444).

Acknowledgment. The work was funded by the Academy of Finland (Project numbers 326444 and 314364) and by the Academy of Finland Flagship Programme, Photonics Research and Innovation (PREIN), decision numbers: 320167 and 320165.

Disclosures. The authors declare no conflicts of interest. T.H. works at Gasera Ltd., which fabricated some of the (commercially available) instrument parts needed in the experiments.

Data availability. Data underlying the results presented in this paper are not publicly available at this time but may obtained from the authors upon reasonable request.

Supplemental document. See Supplement 1 for supporting content.

REFERENCES

1. D. Palaferri, Y. Todorov, A. Bigioli, A. Mottaghizadeh, D. Gacemi, A. Calabrese, A. Vasanelli, L. Li, A. G. Davies, E. H. Linfield, F. Kapsalidis, M. Beck, J. Faist, and C. Sirtori, Nature **556**, 85 (2018).
2. A. Rogalski, Prog. Quantum Electron. **27**, 59 (2003).
3. J. Lehman, A. Sanders, L. Hanssen, B. Wilthan, J. Zeng, and C. Jensen, Nano Lett. **10**, 3261 (2010).
4. K. L. Vodopyanov, in *Laser-based Mid-infrared Sources and Applications* (2020), pp. 247–286.
5. A. N. Baranov, M. Bahriz, and R. Teissier, Opt. Express **24**, 18799 (2016).
6. A. Rogalski, *Infrared Detectors* (CRC Press, 2010).
7. A. Rosencwaig and A. Gersho, J. Appl. Phys. **47**, 64 (1976).
8. G. Wissmeyer, M. A. Pleitez, A. Rosenthal, and V. Ntziachristos, Light: Sci. Appl. **7**, 53 (2018).
9. J. T. Friedlein, E. Baumann, K. A. Briggman, G. M. Colacion, F. R. Giorgetta, A. M. Goldfain, D. I. Herman, E. V. Hoenig, J. Hwang, N. R. Newbury, E. F. Perez, C. S. Yung, I. Coddington, and K. C. Cossel, Nat. Commun. **11**, 3152 (2020).
10. T. Tomberg, M. Vainio, T. Hieta, and L. Halonen, Sci. Rep. **8**, 1848 (2018).
11. P. Patimisco, A. Sampaolo, L. Dong, F. K. Tittel, and V. Spagnolo, Appl. Phys. Rev. **5**, 011106 (2018).
12. J. Karhu, T. Tomberg, F. Senna Vieira, G. Genoud, V. Hänninen, M. Vainio, M. Metsälä, T. Hieta, S. Bell, and L. Halonen, Opt. Lett. **44**, 1142 (2019).
13. M. J. E. Golay, Rev. Sci. Instrum. **18**, 357 (1947).
14. "THz detectors, Microtech Instruments Inc.," retrieved 24 August 2020, http://www.mtinstruments.com/thzdetectors/.
15. O. Ajakaiye, J. Grade, C. Shin, and T. Kenny, Sens. Actuators, A **134**, 575 (2007).
16. K. Hennerich, W. Lahmann, and W. Witte, Infrared Phys. **6**, 123 (1966).
17. M. Naftaly and R. Dudley, Opt. Lett. **34**, 674 (2009).
18. V. Koskinen, J. Fonsen, J. Kauppinen, and I. Kauppinen, Vib. Spectrosc. **42**, 239 (2006).
19. T. Laurila, H. Cattaneo, V. Koskinen, J. Kauppinen, and R. Hernberg, Opt. Express **13**, 2453 (2005).
20. A. Steiger, M. Kehrt, C. Monte, and R. Müller, Opt. Express **21**, 14466 (2013).
21. J. Hodgkinson and R. P. Tatam, Meas. Sci. Technol. **24**, 012004 (2013).
22. G. Leahu, E. Petronijevic, A. Belardini, M. Centini, R. Li Voti, T. Hakkarainen, E. Koivusalo, M. Guina, and C. Sibilia, Sci. Rep. **7**, 2833 (2017).
23. D. C. Fernandez, R. Bhargava, S. M. Hewitt, and I. W. Levin, Nat. Biotechnol. **23**, 469 (2005).
24. N. Radwell, K. J. Mitchell, G. M. Gibson, M. P. Edgar, R. Bowman, and M. J. Padgett, Optica **1**, 285 (2014).
25. J. Rossi, J. Uotila, S. Sharma, T. Laurila, R. Teissier, A. Baranov, E. Ikonen, and M. Vainio, Photoacoustics **23**, 100265 (2021).
26. S. Sharma, T. Laurila, J. Rossi, J. Uotila, M. Vainio, F. Manoocheri, and E. Ikonen, Sens. Actuators, A **337**, 113191 (2022).
27. P. Sievilä, V. P. Rytkönen, O. Hahtela, N. Chekurov, J. Kauppinen, and I. Tittonen, J. Micromech. Microeng. **17**, 852 (2007).
28. C. Lou, H. Chen, X. Li, X. Yang, Y. Zhang, J. Yao, Y. Ma, C. Chang, and X. Liu, Opt. Express **29**, 20190 (2021).
29. Y. Ma, Y. He, P. Patimisco, A. Sampaolo, S. Qiao, X. Yu, F. K. Tittel, and V. Spagnolo, Appl. Phys. Lett. **116**, 011103 (2020).
30. E. Theocharous, C. Engtrakul, A. C. Dillon, and J. Lehman, Appl. Opt. **47**, 3999 (2008).
31. E. Theocharous, R. Deshpande, A. C. Dillon, and J. Lehman, Appl. Opt. **45**, 1093 (2006).
32. E. Theocharous, Metrologia **49**, S99 (2012).

193.51.164.78 {ts '2022-06-01 04:11:25'}